Thermoelectric properties optimization of Fe2VGa by tuning electronic density of states via titanium doping

Pai-Chun Wei, Ta-Sung Huang, Shu-Wei Lin, Guang-Yu Guo, and Yang-Yuan Chen

Citation: Journal of Applied Physics **118**, 165102 (2015); doi: 10.1063/1.4934734
View online: http://dx.doi.org/10.1063/1.4934734
View Table of Contents: http://scitation.aip.org/content/aip/journal/jap/118/16?ver=pdfcov
Published by the AIP Publishing

Thermoelectric properties optimization of Fe_2VGa by tuning electronic density of states via titanium doping

Pai-Chun Wei,[1,a)] Ta-Sung Huang,[1,2] Shu-Wei Lin,[3] Guang-Yu Guo,[3,4] and Yang-Yuan Chen[1,2,a)]
[1]*Institute of Physics, Academia Sinica, 11529 Taipei, Taiwan*
[2]*Graduate Institute of Applied Physics, National Chengchi University, 11605 Taipei, Taiwan*
[3]*Department of Physics, National Taiwan University, 10617 Taipei, Taiwan*
[4]*Physics Division, National Center for Theoretical Sciences, 30013 Hsinchu, Taiwan*

(Received 15 September 2015; accepted 15 October 2015; published online 29 October 2015)

We report the correlation between thermoelectric properties and electronic band structure of thermoelectric Heusler alloy $Fe_2V_{1-x}Ti_xGa$ by comparing experimental measurements with theoretical calculations. The electrical resistivity data show that the semiconducting-like behavior of pure Fe_2VGa is transformed to a more metallic-like behavior at $x = 0.1$. Meanwhile, an enhancement of the Seebeck coefficient was observed for all Ti doped specimens at elevated temperatures with a peak value of 57 μV/K for $x = 0.05$ at 300 K. The experimental results can be elucidated by the calculated band structure, i.e., a gradual shifting of the Fermi level from the middle of the pseudogap to the region of valence bands. With optimized doping, the thermoelectric power factor can be significantly enhanced to 3.95 mW m^{-1} K^{-2} at room temperature, which is comparable to the power factors of Bi_2Te_3-based compounds. The synergy of thermal conductivity reduction due to the alloying effect and the significant increase of the thermoelectric power factor leads to higher order zT values than that of prime Fe_2VGa. © *2015 AIP Publishing LLC*.
[http://dx.doi.org/10.1063/1.4934734]

The Heusler-type intermetallic alloys Fe_2VAl and Fe_2VGa are known as non-magnetic semi-metals exhibiting semiconductor-like behavior, as evidenced by their negative temperature coefficients of resistivity.[1,2] Their semiconductor-like features are attributed to the appearance of a deep pseudogap in the density of states in the vicinity of the Fermi level that is due to the effect of hybridization between *d* and *s-p* states.[3,4] The pseudogap formation implies an indirect band overlap between the electron and hole pockets at the Fermi energy, i.e., a negative band gap $E_g = E_{c,min} - E_{v,max} < 0$, where $E_{c,min}$ and $E_{v,max}$ are the extrema of the conduction and valence bands, respectively. The existence of a pseudogap in Fe_2VAl with a finite density of states at the Fermi level or negative bandgap in the electronic structure has been revealed by optical reflectivity and nuclear magnetic resonance experiments.[5,6] Recent band-structure calculations of Fe_2VAl and Fe_2VGa also revealed the existence of a sharp singularity in the density of state (DOS) near the Fermi level,[7,8] suggesting that both compounds probably have large Seebeck coefficients and would be good candidates for thermoelectric application. Moreover, the low-temperature specific-heat measurements show a huge effective-mass enhancement in both compounds.[9] In general, a semimetal with heavy band mass is expected to have a large Seebeck coefficient.

Several reports have shown that off-stoichiometry or partial substitution can effectively dope electrons or holes to such a Heusler-type system thereby leading to dramatic changes in the electrical resistivity ρ and Seebeck coefficient S.[10–12] Their variations can be understood by means of a rigid band-like Fermi level (E_F) shift from the central region in the pseudogap. In a metallic system, the Seebeck coefficient at temperature T can be written as[11]

$$S(T) = -\frac{\pi^2 k_B^2}{3|e|} T \left(\frac{1}{N(E)} \frac{\partial N(E)}{\partial E} \right)_{E=E_F}, \quad (1)$$

where $N(E)$ is the density of state. A large Seebeck coefficient can be brought about by a low $N(E)$ coupled with its steep slope, $\partial N(E)/\partial E$, at the Fermi level E_F. Through proper carrier doping, the thermoelectric power factor S^2/ρ can be modified and optimized. Much effort has been made to optimize the power factor of Fe_2VAl. For example, a substantial enhancement of the power factor, up to 5.5×10^{-3} W/mK^2, has been found in Sb-substituted Fe_2VAl at room temperature,[10] which is comparable to, and even larger than, the power factors of bulk BiTe-based alloys.[13] This encouraging result makes this material very attractive for thermoelectric applications.

The thermoelectric performance of a material can usually be evaluated by using the dimensionless figure of merit defined as $zT = (S^2/\rho\kappa)T$, where κ is the total thermal conductivity. In 2002, Lue and Kuo showed that the undoped Fe_2VGa might exhibit better thermoelectric performance than Fe_2VAl,[14] mainly due to its one-order higher electrical conductivity, 20% lower thermal conductivity, and similar Seebeck coefficient. In this work, the electronic structure and thermoelectric-related properties of Ti-substituted Fe_2VGa are investigated. The calculated band-structures show the existence of a pseudogap and sharp DOS edges adjacent to it. The calculated band structures are further examined by probing the electrical resistivity and Seebeck coefficient, both of which are very sensitive to the details of the Fermi

[a)]pcwei68@gmail.com and cheny2@phys.sinica.edu.tw

surface. The alloying effect on lattice thermal conductivity by Ti substitution is also examined.

Ingots of $Fe_2V_{1-x}Ti_xGa$ with nominal compositions of $x = 0$, 0.05, 0.1, 0.15, 0.2, 0.25 were prepared by repeated arc melting of pure Fe (99.9%), V (99.7%), Ga (99.9999%), Ti (99.5%) elements in an argon atmosphere. The ingots were homogenized at 1273 K for 72 h in an evacuated quartz capsule followed by furnace cooling. Their actual chemical compositions were then determined by energy dispersive x-ray spectroscopy (EDX). The electrical resistivity and Seebeck coefficient were measured by an ULVAC ZEM-3 system. The thermal diffusivity of samples was measured on a NETZSCH LFA 457 laser flash instrument. The thermal conductivity was then calculated from the relationship $\kappa = \alpha C_p d$, where α is the thermal diffusivity, C_p is the heat capacity according to the Dulong-Petit law, and d is the mass density, measured by Archimedes' method.

We have performed self-consistent electronic structure calculations for $Fe_2V_{1-x}Ti_xGa$ Heusler alloys within the density functional theory with the local density approximation (LDA). We used an accurate full-potential linearized augmented plane wave (FLAPW) method, as implemented in the WIEN2K code.[15] The wave function, charge density, and potential were expanded in terms of the spherical harmonics inside the muffin-tin spheres. The cutoff angular moments (L_{max}) used were 10, 6, and 6, respectively. The wave function outside the muffin-tin spheres is expanded in terms of the augmented plane waves (APWs) and a large number of APWs (~70 APWs/atom, i.e., the maximum size of the crystal momentum $K_{max} = 8/R_{mt}$) were included in the present calculations. To obtain accurate electronic band structures, a fine $27 \times 27 \times 27$ grid with 1470 k-points in the irreducible Brillouin zone wedge (IBZW) is used. We consider the $Fe_2V_{1-x}Ti_xGa$ Heusler alloys to be in fully ordered cubic $L2_1$ structure. The alloying effect was simulated by using the virtual crystal approximation (VCA). In the present VCA calculations, the V/Ti site is replaced by a virtual atom with the atom number $Z = (1-x)Z_V + xZ_{Ti}$, where Z_V and Z_{Ti} are the V and Ti atomic numbers, respectively, and x is the Ti composition. Experimental lattice constants are used for all considered Heusler alloys.

Fig. 1(a) shows the overall XRD patterns for Ti-substituted $Fe_2V_{1-x}Ti_xGa$ with $x = 0$–0.25, which essentially remain unaltered upon replacement of V by Ti. All of them are identified as Heusler-type $L2_1$ structures, with no trace of other phases. The corresponding lattice parameters of the $L2_1$ phase as a function of doping content are given in Fig. 1(b). Clearly, the lattice parameters for the Ti substitution increase linearly with the composition x. This indicates that the V sites are replaced by Ti atoms in the well-ordered $L2_1$ Heusler phase. Their actual compositions have also been checked using EDX and found to be compositionally accurate within the limit of EDX (<5%).

Fig. 2(a) shows the calculated energy bands of stoichiometry Fe_2VGa. At $x = 0$, there are four bands crossing E_F including three degenerate hole pocket sheets of the Fermi surface centered at the Γ point, formed by the intersection of E_F with the valence band along symmetry lines L-Γ-X, and an electron Fermi surface section centered at the X point

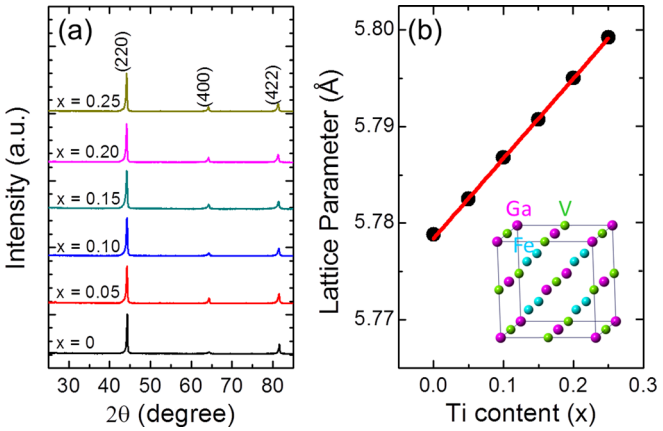

FIG. 1. (a) X-ray diffraction patterns and (b) lattice parameters for $Fe_2V_{1-x}Ti_xGa$ ingot specimens for various x. The line represents linear fit. The inset shows the crystal structure of Fe_2VGa.

formed by the intersection of E_F with the conduction band along symmetry lines Γ-X-W, with nearly the same effective mass. This indirect overlap between the hole and electron pockets infers electron and hole carrier compensation,

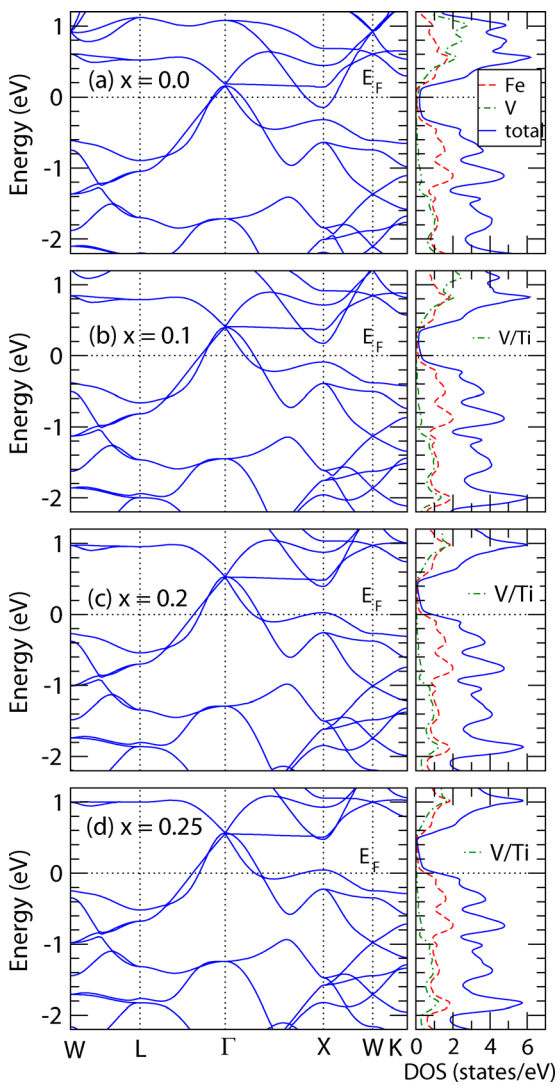

FIG. 2. Band structure as well as total and site-decomposed density of states (DOS) of $Fe_2V_{1-x}Ti_xGa$ with $x = 0$–0.25. E_F denotes the Fermi level (0 eV).

thereby giving rise to a very small net number of carriers in Fe_2VGa, as evidenced by NMR relaxation and Hall-effect measurements.[6,16] Figs. 2(b)–2(d) present the energy bands for Ti doping levels of $x = 0.10$, 0.20, and 0.25, respectively. The appreciable downward shift of the Fermi level with increase in x can be attributed to the increase in hole carriers via substitution, since Ti ($[Ar]3d^24s^2$) has one less electron in its valence shell than V ($[Ar]3d^34s^2$).

The calculated total and partial atomic (Fe,V) DOSs for Fe_2VGa are also shown in Fig. 2(a). The total DOS has a pseudogap near E_F due to the carrier compensation and sharp DOS edges at ~0.05 eV in the conduction band and at −0.3 eV in the valence band. From the partial DOS calculation, the sharp edges mainly originate from Fe-*d* states. Note that the partial DOSs of Ga are not shown here because of their negligible contribution. The pseudogap feature is believed to be responsible for the semiconducting-like behavior in the electrical resistivity in Fe_2VGa. Figs. 2(b)–2(d) show the total and partial atomic (Fe,V/Ti) DOSs for Ti-substituted $Fe_2V_{1-x}Ti_xGa$ ($x = 0.1$, 0.2, 0.25). Clearly, the Fermi level is shifted toward valence band as V is substituted by Ti. It is noteworthy that when x reaches 0.2 the Fermi level intersects with the DOS up turning point. This dramatic rise in DOS is contributed not only from the hole bands along L-Γ-X but also from the newly formed hole Fermi surface along Γ-X-W, as shown in Fig. 2(c). The sharp slope in DOS at the Fermi level is an important feature of a large Seebeck coefficient.

Fig. 3(a) shows the temperature dependence of electrical resistivity $\rho(T)$ for $Fe_2V_{1-x}Ti_xGa$. Apparently, the substitution of Ti onto V sites effectively reduces the electrical resistivity of $Fe_2V_{1-x}Ti_xGa$ due to the increase of valence electron numbers. For $x = 0$ and 0.05 samples, the $\rho(T)$'s show upturns near room temperature, indicating that both of them possess semiconducting-like behavior at lower temperature. Above 300 K, their temperature coefficients of resistivities are found to be positive. Such observations could be attributed to the slight excess of Ga.[17] For $x \geq 0.1$ samples, the $\rho(T)$'s become lower and show traditional metallic behavior. This can be explained by means of the Fermi level shift as mentioned in Fig. 2. Since the DOS within the pseudogap is very small, a small change in the electron/hole concentration could result in an appreciable shifting of the Fermi level. For example, the Fermi energy shifts 0.15 eV as Ti content varies only 0.05 at. %.

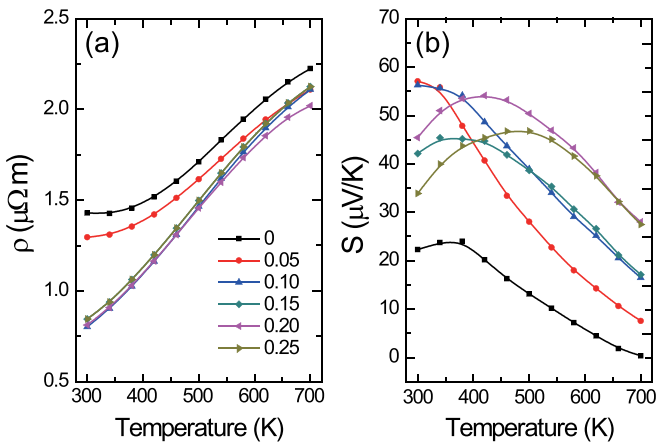

FIG. 3. (a) Temperature dependence of electrical resistivity ρ and (b) Seebeck coefficient S for $Fe_2V_{1-x}Ti_xGa$ with $x = 0$–0.25.

The temperature dependence of Seebeck coefficient $S(T)$ for $Fe_2V_{1-x}Ti_xGa$ is shown in Fig. 3(b). For Fe_2VGa, as temperature increases the Seebeck coefficient increases from 22 μV/K at 300 K to a maximum S_{max} of 25 μV/K near 400 K, followed by a reduction approaching zero. The positive values in the entire temperature range indicate that the hole is the dominant carrier in the prime compound. This result is consistent with the calculated energy bands depicted in Fig. 2(a), which shows the existence of a relatively large hole Fermi surface. For $x = 0.05$, the S_{max} value dramatically increases to 57 μV/K and the whole S curve shifts to more than two times higher than that of prime Fe_2VGa. It is known that the Seebeck coefficient is a sensitive probe of energy relative to the Fermi surface and can be expressed as[18]

$$S = \left(\frac{\sigma_p S_p + \sigma_n S_n}{\sigma_p + \sigma_n}\right), \tag{2}$$

where $S_{p,n}$ and $\sigma_{p,n}$ represent the Seebeck coefficients and electrical conductivities for the *p*- and *n*-type carriers, respectively. Such a large enhancement of S can be attributed to the substantial downward shift of E_F from the center of the pseudogap to just beneath the extremum of the electron pocket at the X point, leaving the framework of two-carrier electrical conduction. The S curve of the $x = 0.1$ sample upsurges further, especially at elevated temperatures. As depicted in Fig. 2(b), E_F leaving the electron pocket suppresses the thermal excitation of electrons, and results in the enhancement of S in the higher temperature region. Compared with the $x = 0.1$ sample, the $x = 0.15$ sample has lower S values near room temperature but slightly higher S values in the higher temperature region, 460–700 K. The S_{max} value reduces to 45 μV/K at 340 K. It is known that the S value is inversely proportional to $N(E)$ and proportional to its slope $\partial N(E)/\partial E$ at the Fermi level, as expressed in Eq. (1). The further increase in Ti doping level, from $x = 0.1$ to $x = 0.15$, increases the total $N(E)$ near E_F, but its slope is almost unchanged. This causes S curve and S_{max} values to decrease. When $x = 0.2$, the S curve again upsurges and the S_{max} value achieves ~55 μV/K at 420 K. As shown in Fig. 2(c), the Fermi level E_F intersects with a high DOS slope and leads to a significant enhancement in the S value, because of the newly formed hole Fermi surface along Γ-X-W. When x further increases to 0.25, the S curve and S_{max} values drop due to the higher $N(E)$ but similar $\partial N(E)/\partial E$ at E_F, as depicted in Fig. 2(d). From Eq. (1), the S value is proportional to the temperature; however, the S curves of all samples go down with temperature increase after passing through the maximum Seebeck coefficient S_{max}. This can also be found in Fe_2VAl Heusler systems in both *p*- and *n*-type dopant specimens. It is obvious that the temperature of S_{max} shifts to higher temperature and the S curve becomes more flat as Ti content increases. This is a clear indication of less thermally excited electrons which jump across the energy gap and compensate with positive carriers, due to the lowering E_F.

To evaluate the thermoelectric performance of $Fe_2V_{1-x}Ti_xGa$, the thermal conductivity κ is measured from 300 to 700 K as shown in Fig. 4(a). The thermal conductivity gradually decreases with increasing temperature for all alloys. Moreover, the $\kappa(T)$ curve decreases with increasing Ti content. To clarify the origin of the reduction in $\kappa(T)$, the lattice thermal conductivity κ_L is estimated by $\kappa_L = \kappa - \kappa_e$. The electronic thermal conductivity κ_e can be evaluated using the Wiedemann-Franz law $\kappa_e\rho/T = L_0$, where $L_0 = 2.45 \times 10^{-8}\,W\,\Omega\,K^{-2}$ is the Lorentz number. As shown in Fig. 4(b), κ_L decreases about 80% as $x = 0.25$, indicating an enhanced phonon scattering due to alloying effect of Ti substitution for V. It is noticed that although the κ_L curve of the $x = 0.1$ sample is lower than that of the $x = 0.05$ sample near room temperature, $\kappa(T)$ is almost the same at elevated temperatures. This result indicates that the carrier contribution to the thermal conductivity would be very significant while the Fermi level leaves the pseudogap in the Ti doped $Fe_2V_{1-x}Ti_xGa$ Heusler system.

Fig. 4(c) shows the temperature dependence of power factor $(S^2/\rho)$of the various samples. All of the Ti-substituted $Fe_2V_{1-x}Ti_xGa$ samples show a larger power factor than that of prime Fe_2VGa because of their lower electrical resistivities and higher Seebeck coefficients. As $x = 0.1$ ($Fe_2V_{0.9}Ti_{0.1}Ga$), the power factor reaches 3.95 $mW\,m^{-1}\,K^{-1}$ at room temperature. This value is compatible to the power factors of Bi-Te based compounds,[13] Fe$_2$VAl-based alloys,[12] and $Sr_{1-x}La_xTiO_3$ metallic perovskites,[19] the known large power factor materials near room temperature, and is about 50% higher than the power factor of the similar Heusler compound $Fe_2V_{0.9}Ti_{0.1}Al$.[20,21] At 340 K, the power factor decreases to 2.2 $mW\,m^{-1}\,K^{-1}$ at $x = 0.15$ because of the lower Seebeck coefficient, it then increases again to 2.9 $mW\,m^{-1}\,K^{-1}$ as x further increases to 0.2, due to the dramatic rise in DOS contributed from the hole Fermi surface near the X point. Fig. 4(d) gives the temperature dependence of zT calculated from the measured values of ρ, S, and κ_{tot}. Significantly, an upshift zT curve can be achieved by increasing Ti concentration. This is mainly due to the simultaneous increase of σ and S with lowering κ. The highest zT is 0.07 at 420 K for $x = 0.2$, which is a 12-fold increase between prime Fe_2VGa and $Fe_2V_{0.8}Ti_{0.2}Ga$. However, the value is still an order of magnitude smaller than those of state-of-the-art thermoelectric materials such as Bi_2Te_3. It is worth mentioning that the alloying of heavier atoms in such a Heusler alloy could reduce the lattice thermal conductivity due to the enhancement of phonon scattering. With the success of thermoelectric power factor optimization by shifting Fermi surface, we believe the substitution of heavier atoms has great potential for investigating the possible enhancement of thermoelectric performance in this class of materials. Fig. 5 gives the temperature dependence of compatibility factor s of $Fe_2V_{1-x}Ti_xGa$, an indicator of rational materials selection and device design for segmented generators. Generally, if the compatibility factors of the segmented materials differ by a factor of two or more, the device efficiency will be substantially reduced.[22] With increasing Ti concentration, the compatibility factor s of $Fe_2V_{1-x}Ti_xGa$ increases monotonically and attains 1 to 2 near room temperature, which is compatible to current high-performance p-type Zintl phase thermoelectrics such as $EuZn_2Sb_2$ and $Yb_{14}MnSb_{11}$.[22,23]

In conclusion, a strong correlation between electrical conductivity, Seebeck coefficient, band structure, and density of state is revealed in Ti-substituted Fe_2VGa through the combination of theoretical calculations and experimental measurements. Upon Ti substitution, the electron/hole pockets near the band edges are modified and the Fermi energy E_f downshifts, leaving the extrema of the conduction band at $x = 0.1$ and intersecting with an additional hole pocket at

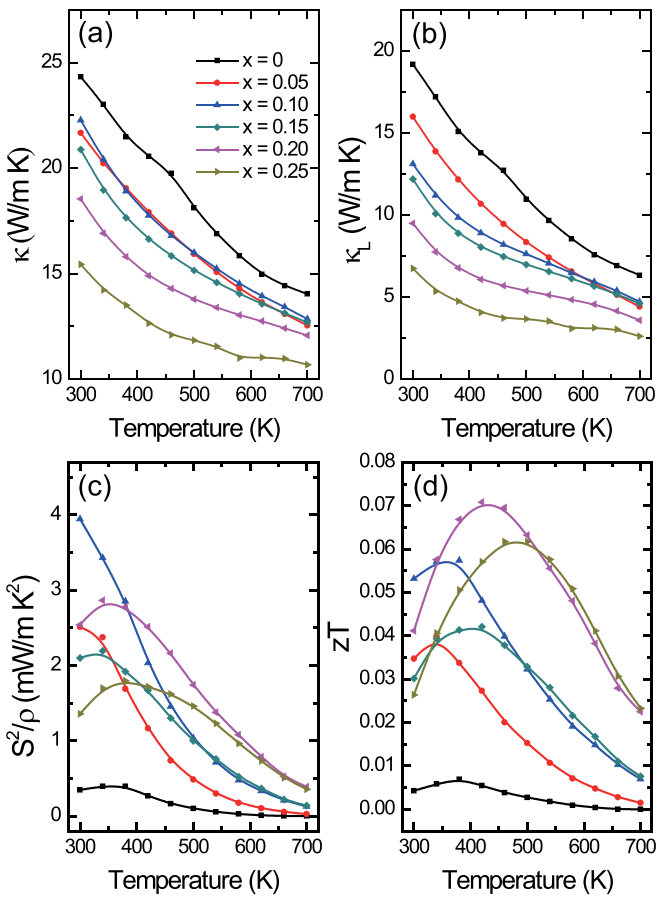

FIG. 4. (a) Temperature dependence of total thermal conductivity κ, (b) lattice thermal conductivity κ_L, (c) power factor S^2/ρ, and (d) zT for $Fe_2V_{1-x}Ti_xGa$ with $x = 0$–0.25.

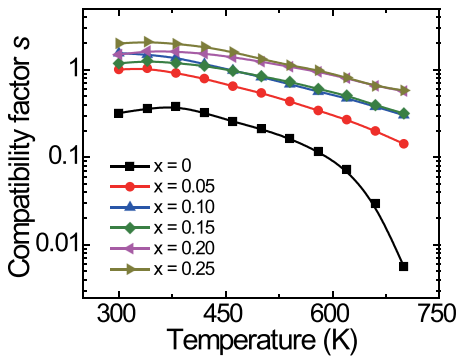

FIG. 5. Temperature dependence of compatibility factor s for $Fe_2V_{1-x}Ti_xGa$ with $x = 0$–0.25.

$x = 0.2$. The electrical resistivity and Seebeck coefficient are found to be very sensitive to the Fermi surfaces, determined by the content of carrier doping. The suppression of carrier compensation and the intersection of E_F with a high DOS slope lead to a significant enhancement of the Seebeck coefficient. Meanwhile, the suppression of thermal excitation results in a slowed decrease of the Seebeck coefficient at higher temperature and, consequently, a more flattening temperature-dependent S curve. The synergy of the thermal conductivity reduction due to the alloying of Ti into V and the significant increase of the thermoelectric power factor leads to higher zT values than that of prime Fe_2VGa.

The authors would like to thank the Minister of Science and Technology in Taiwan for financial supports. We are grateful to Dr. Chien-Chih Yeh and the Center for Measurement Standards, Industrial Technology Research Institute in Taiwan for technical support.

[1]Y. Nishino, M. Kato, S. Asano, K. Soda, M. Hayasaki, and U. Mizutani, Phys. Rev. Lett. **79**, 1909 (1997).
[2]N. Kawamiya, Y. Nishino, M. Matsuo, and S. Asano, Phys. Rev. B **44**, 12406 (1991).
[3]G. Y. Guo, G. A. Botton, and Y. Nishino, J. Phys.: Condens. Matter **10**, L119 (1998).
[4]A. Bansil, S. Kaprzyk, P. E. Mijnarends, and J. Toboła, Phys. Rev. B **60**, 13396 (1999).
[5]H. Okamura, J. Kawahara, T. Nanba, S. Kimura, K. Soda, U. Mizutani, Y. Nishino, M. Kato, I. Shimoyama, H. Miura, K. Fukui, K. Nakagawa, H. Nakagawa, and T. Kinoshita, Phys. Rev. Lett. **84**, 3674 (2000).
[6]C. S. Lue and J. H. Ross, Jr., Phys. Rev. B **58**, 9763 (1998).
[7]C. Venkatesh, V. Srinivas, V. V. Rao, S. K. Srivastava, and P. S. Babu, J. Alloys Compd. **577**, 417 (2013).
[8]A. Ślebarski and J. Goraus, Phys. Rev. B **80**, 235121 (2009).
[9]C. S. Lue, J. H. Ross, Jr., C. F. Chang, and H. D. Yang, Phys. Rev. B **60**, R13941 (1999).
[10]M. Mikami, S. Tanaka, and K. Kobayashi, J. Alloys Compd. **484**, 444 (2009).
[11]Y. Nishino, S. Deguchi, and U. Mizutani, Phys. Rev. B **74**, 115115 (2006).
[12]Y. Nishino and Y. Tamada, J. Appl. Phys. **115**, 123707 (2014).
[13]W. J. Xie, S. Y. Wang, S. Zhu, J. He, X. F. Tang, Q. J. Zhang, and T. M. Tritt, J. Mater. Sci. **48**, 2745 (2013).
[14]C. S. Lue and Y. K. Kuo, Phys. Rev. B **66**, 085121 (2002).
[15]P. Blaha, K. Schwarz, G. Madsen, D. Kvasnicka, and J. Luitz, *WIEN2k, An Augmented Plane Wave Local Orbitals Program for Calculating Crystal Properties* (Technische University Wien, Austria, 2001).
[16]T. Fukuhara, H. Matsuda, S. Masubuchi, K. Ooiwa, Y. Takano, F. Shimizu, and K. Endo, J. Phys. Soc. Jpn. **73**, 13 (2004).
[17]C. S. Lue, W. J. Lai, C. C. Chen, and Y. K. Kuo, J. Phys.: Condens. Matter **16**, 4283 (2004).
[18]C. S. Lue, C. F. Chen, J. Y. Lin, Y. T. Yu, and Y. K. Kuo, Phys. Rev. B **75**, 064204 (2007).
[19]T. Okuda, K. Nakanishi, S. Miyasaka, and Y. Tokura, Phys. Rev. B **63**, 113104 (2001).
[20]H. Matsuura, Y. Nishino, U. Mizutani, and S. Asano, J. Jpn. Inst. Met. **66**, 767 (2002).
[21]Y. Nishino, in *The Science of Complex Alloy Phases*, edited by T. B. Massalski and P. E. Turchi (TMS, Warrendale, 2005), p. 325.
[22]G. J. Snyder and T. S. Ursell, Phys. Rev. Lett. **91**, 148301 (2003).
[23]H. Zhang, M. Baitinger, M. B. Tang, Z. Y. Man, H. H. Chen, X. X. Yang, Y. Liu, L. Chen, Y. Grin, and J. T. Zhao, Dalton Trans. **39**, 1101 (2010).